www.czasopisma.pan.pl PAN POLSKA AKADEMIA NAUK www.journals.pan.pl

Arch. Min. Sci. **63** (2018), 1, 183-204

Electronic version (in color) of this paper is available: http://mining.archives.pl

DOI 10.24425/118894

PIOTR CHELUSZKA*#, ROMAN KAULA**,
ADAM HEYDUK**, JACEK GAWLIK*

MODELLING THE DYNAMICS OF A DRIVE OF BOOM-TYPE ROADHEADER CUTTING HEADS AT ADJUSTABLE ANGULAR SPEED

MODELOWANIE DYNAMIKI NAPĘDU GŁOWIC URABIAJĄCYCH WYSIĘGNIKOWEGO KOMBAJNU CHODNIKOWEGO Z REGULOWANĄ PRĘDKOŚCIĄ KĄTOWĄ

The article presents a dynamic model of a drive system of cutting heads of a boom-type roadheader equipped with an inverter system. Such roadheaders are used in underground mining for the mechanised drilling of roadways and for tunnelling in civil engineering. If the created mathematical model takes into account the electromagnetic effects accompanying the work of an asynchronous motor and an adjustable source of the motor power supply (inverter), dynamic effects can be simulated in the drive system working at different, angular velocities of cutting heads with stepless adjustment. The created mathematical model was implemented in Matlab/Simulink environment. The so established simulation model allows to perform numerical investigations, in particular for the purpose of optimisation of the values of the cutting process parameters, including the selection of cutting heads' angular speed in the aspect of reducing dynamic loads and minimising the energy consumption of the cutting process. The representation of the inverter system dynamics allows to analyse the dynamic loads of all the key elements of the drive of the cutting heads – a drive motor, the parts of the system of power transmission onto cutting heads, equipped with a multistage transmission gear, and (allows) to examine the behaviour of an inverter system in its different operational modes.

Keywords: roadheader, cutting system, inverter system, speed adjustment, mathematical model, dynamics simulation

W artykule przestawiono model dynamiczny układu napędowego głowic urabiających wysięgnikowego kombajnu chodnikowego wyposażonego w układ przekształtnikowy. Kombajny tego rodzaju stosowane są w górnictwie do zmechanizowanego drążenia wyrobisk korytarzowych oraz tuneli w budownictwie inżynieryjnym. Uwzględnienie w opracowanym modelu matematycznym zjawisk elektromagentycznych

* SILESIAN UNIVERSITY OF TECHNOLOGY, FALCULTY MINING AND GEOLOGY, DEPARTMENT OF MINING MECHANIZATION AND ROBOTISATION, 2 AKADEMICKA STR., 44-100 GLIWICE, POLAND

** SILESIAN UNIVERSITY OF TECHNOLOGY, FACULTY OF MINING AND GEOLOGY, DEPARTMENT OF ELECTRICAL ENGINEERING AND INDUSTRIAL AUTOMATION, 2 AKADEMICKA STR., 44-100 GLIWICE, POLAND

Corresponding author: Piotr.Cheluszka@polsl.pl

towarzyszących pracy silnika asynchronicznego oraz sterowanego źródła zasilania silnika (falownika) pozwala na symulowanie zjawisk dynamicznych w układzie napędowym pracującym przy różnych, regulowanych bezstopniowo prędkościach kątowych głowic urabiających. Utworzony model matematyczny został zaimplementowany w środowisku Matlab/Simulink. Uzyskany w ten sposób model symulacyjny pozwala na realizację badań numerycznych, między innymi dla potrzeb optymalizacji wartości parametrów procesu urabiania, w tym doboru prędkości kątowej głowic urabiających w aspekcie redukcji obciążeń dynamicznych i minimalizacji energochłonności procesu urabiania. Odwzorowanie dynamiki układu przekształtnikowego umożliwia analizę obciążeń dynamicznych wszystkich kluczowych elementów napędu głowic urabiających – silnika napędowego, elementów układu przeniesienia napędu na głowice urabiające wyposażonego w wielostopniową przekładnię zębatą oraz badanie zachowania się układu przekształtnikowego w różnych stanach jego pracy.

Słowa kluczowe: kombajn chodnikowy, układ urabiania, układ przekształtnikowy, regulacja prędkości, model matematyczny, symulacja dynamiki

1. Introduction

The mechanised drilling of roadways and tunnelling in underground mines is based on the use of roadheaders. These are unit construction machines performing the main technological operations, namely: mechanical rock excavation, loading the mined rock onto the means of transport, transporting the mined rock from the heading face and the execution of the excavation support. Rock mining is, however, the principal task of this type of machines. Mechanical rock cutting in heading works carried out in underground mining is performed by cutting with picks mounted in pickboxes welded to the side surface of a cutting head. Boom-type roadheaders belong to the group of roadheaders mining this way (Fig. 1). A cutting system in this case has the form of a mobile boom at the end of which one longitudinal or two transverse cutting

Fig. 1. R-130 boom-type roadheader (manufactured by Famur S.A.) on the test station at the Technology Hall of Faculty of Mining and Geology, Silesian University of Technology, Gliwice, Poland

heads with small dimensions in relation to the cross section field of the roadways or tunnel being drilled are mounted. Such heads are put into rotary motion around their axis of rotation by a drive system and are additionally moved along the heading face surface as a result of boom deflection in the plane parallel and perpendicular to the floor. Headings with any shape and cross section size can be excavated this way. The cutting system, due to the function it performs, is therefore a key component of a mining machine critical to its operational performance and efficiency.

The rock cutting process being performed is causing strong vibration excitations and dynamic loads in the cutting system, which are transmitted through a load-carrying structure onto other roadheader subassemblies. The drive of the cutting heads and their load-carrying structure (boom) should be distinguished in the construction of the cutting system of the boom-type roadheader. The issue of modelling the dynamics of the roadheader boom is described, for example, in these works: (Dolipski et al., 2014; Wang et al., 2015). The issue of the dynamics of a drive of the cutting heads of the boom-type roadheader was already discussed earlier (e.g. (Dolipski & Cheluszka, 1999; Kessler et al., 1989; Wei & Xie, 2012)). The simulation tests performed so far – based on the created mathematical models – covered mainly, however, the dynamic effects occurring in the system itself of power transmission from an electric motor onto cutting heads subjected to the activity of vibrations' excitation from mining. A drive motor, as a torque referencing unit, was considered here in a simplified way. A mathematical model of an asynchronous motor, used commonly for such type of drives, was based on the use of a static characteristic linking of the torque reached by a motor with its rotor's angular speed (the electromagnetic phenomena existing there were omitted) (Dolipski, 1993). Such an approach has been fully sufficient until now. The work of cutting heads in the predefined states was only investigated. The natural mechanical characteristics of drive systems could be used in modelling of dynamic loads in a drive of roadheader cutting heads also because in the roadheaders produced until now, such motors are supplied directly from a power supply network. For this reason, cutting is carried out with one or with one of two, for two-speed motors, angular speeds of cutting heads.

The angular speed of cutting heads should be adjusted to rock workability. It is assumed that the less workable the rock is, the lower should be the speed. This is advantageous considering the energy consumption of mining and pick wear intensity. Mining practice has shown that the rock workability varies. Rocks with identical properties are rarely deposited in the cross section of the drilled heading or tunnel. Alternate configurations of rock layers, which are hard and easy to work, exist if we look at a geological structure of the rock mass. The experimental and simulation investigations of the roadheader mining process conducted for many years in the Department of Mining Mechanization and Robotisation of the Faculty of Mining and Geology, Silesian University of Technology, have led to a conclusion that freely adjustable angular speed of cutting heads, depending on the properties of the worked rock, will be advantageous (Dolipski et al., 2015). The most convenient method of adjusting this speed is to use an inverter. Hence the need to develop a dynamic model of a cutting heads drive equipped with a converter system enabling to adjust their angular speed. This work presents a dynamic model of a drive of cuttings heads of a boom-type roadheader, R-130 (by Famur S.A.), equipped with a converter system (experimental installation). The roadheader, with the mass of about 30 t and the cutting system power of 132 kW, is the basic type of a roadheader used in heading works in the Polish hard coal industry. The model was implemented in the Matlab/Simulink environment for the purpose of simulation tests. This allows to analyse the dynamics of a converter drive of cutting

heads: an electric motor supplied from a controlled power supply source (inverter) and a power transmission system. For this reason, the drive of cutting heads is considered here as a class of mechatronic facilities (Bishop, 2002).

2. Dynamic model of a drive of cutting heads with adjustable angular speed

Two sub-systems are distinguished in the structure of a dynamic model of a drive of boom-type roadheader cutting heads: a mechanical system transmitting power from an electric motor onto cutting heads and an electrical converter system connected to an asynchronous double squirrel-cage drive motor.

2.1. Modelling the dynamics of the power transmission system

A system of power transmission from a drive motor onto boom-type roadheader cutting heads is a classical mechanical system comprising an electric motor, a coupling (usually a flexible coupling), a multistage toothed gear and a working unit – cutting heads in this case. The drive construction consists of rotating parts such as discs, in which their mass is concentrated, connected with shafts. This allows to build a physical model with a discrete structure, which considerably simplifies a mathematical description of motion (Bishop, 2002). The structure of a physical model of a drive of cutting heads will mainly depend on the toothed gear construction (the type and number of stages) distinct for the given roadheader type. A kinematic diagram of the considered drive is shown in Fig. 2a. As it is possible to measure dynamic loads during experimental tests on a test station, the drive of the R-130 roadheader cutting heads was equipped with an additional flexible coupling allowing to attach a torque metre (MI) between a drive motor and a toothed gear.

The created physical model of a system of power transmission from a motor to cutting heads has fifteen degrees of freedom (Fig. 2b). This represents a kinematic system of a three-stage, two-way bevel-cylindrical gear applied in the above roadheader. Torsionally vibrating masses with the moment of inertia I_M, $I_K^{(11)}$, $I_K^{(12)}$,..., $I_G^{(1)}$, $I_G^{(2)}$ are connected with weightless viscoelastic elements modelling elastic and damping properties of shafts, couplings and meshing of toothed gears. Such elements are characterised by specific torsional rigidity k_{MK}, $k_K^{(1)}$, k_{MI},..., $k_{6G}^{(1)}$, $k_{6G}^{(2)}$. On the other hand, their damping properties are described with the damping coefficients c_{MK}, $c_K^{(1)}$, c_{MI},..., $c_{6G}^{(1)}$, $c_{6G}^{(2)}$. The temporary location of the distinguished masses is described with the angular coordinates: φ_M, $\varphi_K^{(11)}$, $\varphi_K^{(12)}$,..., $\varphi_G^{(1)}$, $\varphi_G^{(2)}$. A physical model of the cutting heads drive is subject to the activity of vibration excitations in the form of the moment of load force of the left cutting head ($M_{OB}^{(1)}$) and right cutting head ($M_{OB}^{(2)}$) generated by the process of cutting a heading face of the drilled roadways.

Motion equations in the developed discrete physical model were entered using a Lagrange second degree equation (Hand & Finch, 1998). A mathematical model describing the movement of masses creates a system of fifteen ordinary second-order differential equations, which have the following form in the matrix-vector form:

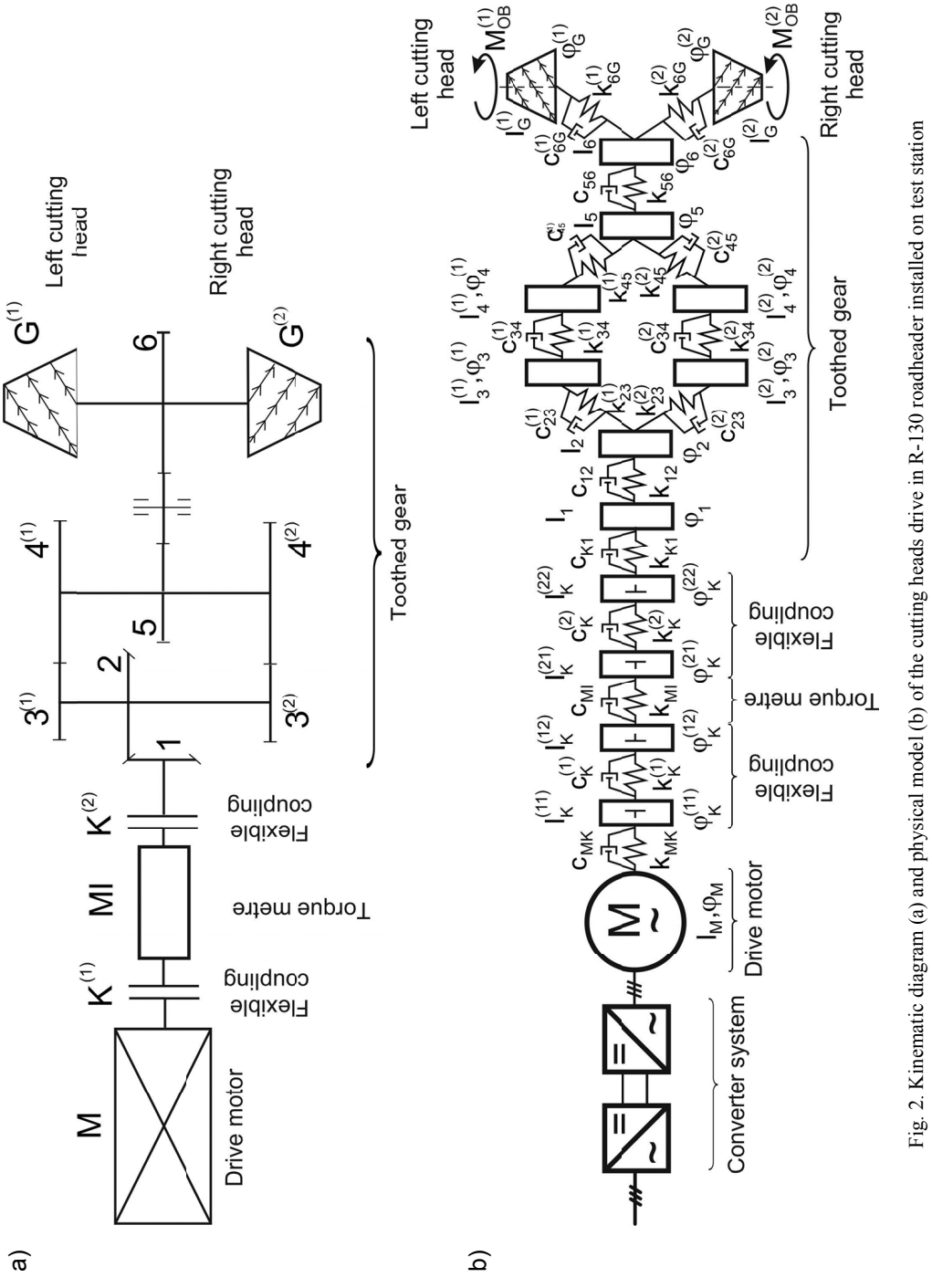

Fig. 2. Kinematic diagram (a) and physical model (b) of the cutting heads drive in R-130 roadheader installed on test station

$$\mathbf{J}\cdot\ddot{\mathbf{q}}+\mathbf{C}\cdot\dot{\mathbf{q}}+\mathbf{K}\cdot\mathbf{q}=\mathbf{Q} \tag{1}$$

where:

- $\mathbf{J}$ — matrix of inertia;
- $\mathbf{C}$ — matrix of damping;
- $\mathbf{K}$ — matrix of rigidity;
- $\mathbf{Q}$ — vector of external load;
- $\mathbf{q}, \dot{\mathbf{q}}, \ddot{\mathbf{q}}$ — vectors of coordinates and their successive derivatives.

The matrix of inertia assumes the following form:

$$\mathbf{J}=\begin{bmatrix}
I_M & 0 & 0 & 0 & 0 & 0 & 0 & 0 & 0 & 0 & 0 & 0 & 0 & 0 \\
0 & I_K^{(11)} & & & & & & & & & & & & 0 \\
0 & & I_K^{(12)} & & & & & & & & & & & 0 \\
0 & & & I_K^{(21)} & & & & & & & & & & 0 \\
0 & & & & I_K^{(22)} & & & & & & & & & 0 \\
0 & & & & & I_1 & & & & & & & & 0 \\
0 & & & & & & I_2 & & & & & & & 0 \\
0 & & & & & & & I_3^{(1)} & & & & & & 0 \\
0 & & & & & & & & I_4^{(1)} & & & & & 0 \\
0 & & & & & & & & & I_3^{(2)} & & & & 0 \\
0 & & & & & & & & & & I_4^{(2)} & & & 0 \\
0 & & & & & & & & & & & I_5 & & 0 \\
0 & & & & & & & & & & & & I_6 & 0 \\
0 & & & & & & & & & & & & & I_G^{(1)} \\
0 & 0 & 0 & 0 & 0 & 0 & 0 & 0 & 0 & 0 & 0 & 0 & 0 & I_G^{(2)}
\end{bmatrix} \tag{2}$$

Whereas the matrix of damping and the matrix of rigidity assumes the forms designated, respectively, as: (3) and (4).

$$\mathbf{C}=\begin{bmatrix}
c_{1,1} & c_{1,2} & 0 & 0 & 0 & 0 & 0 & 0 & 0 & 0 & 0 & 0 & 0 & 0 & 0 \\
c_{2,1} & c_{2,2} & c_{2,3} & 0 & 0 & & & & & & & & & & 0 \\
0 & c_{3,2} & c_{3,3} & c_{3,4} & 0 & 0 & & & & & & & & & 0 \\
0 & 0 & c_{4,3} & c_{4,4} & c_{4,5} & 0 & 0 & & & & & & & & 0 \\
0 & 0 & 0 & c_{5,4} & c_{5,5} & c_{5,6} & 0 & 0 & & & & & & & 0 \\
0 & & 0 & 0 & c_{6,5} & c_{6,6} & c_{6,7} & 0 & 0 & & & & & & 0 \\
0 & & & 0 & 0 & c_{7,6} & c_{7,7} & c_{7,8} & 0 & c_{7,10} & & & & & 0 \\
0 & & & & 0 & 0 & c_{8,7} & c_{8,8} & c_{8,9} & 0 & 0 & & & & 0 \\
0 & & & & & 0 & 0 & c_{9,8} & c_{9,9} & 0 & 0 & c_{9,12} & & & 0 \\
0 & & & & & & c_{10,7} & 0 & 0 & c_{10,10} & c_{10,11} & 0 & 0 & & 0 \\
0 & & & & & & & 0 & 0 & c_{11,10} & c_{11,11} & c_{11,12} & 0 & 0 & 0 \\
0 & & & & & & & & c_{12,9} & 0 & c_{12,11} & c_{12,12} & c_{12,13} & 0 & 0 \\
0 & & & & & & & & & 0 & 0 & c_{13,12} & c_{13,13} & c_{13,14} & c_{13,15} \\
0 & & & & & & & & & & 0 & 0 & c_{14,13} & c_{14,14} & 0 \\
0 & 0 & 0 & 0 & 0 & 0 & 0 & 0 & 0 & 0 & 0 & 0 & c_{15,13} & 0 & c_{15,15}
\end{bmatrix} \tag{3}$$

$$\mathbf{k} = \begin{bmatrix}
k_{1,1} & k_{1,2} & 0 & 0 & 0 & 0 & 0 & 0 & 0 & 0 & 0 & 0 & 0 & 0 & 0 \\
k_{2,1} & k_{2,2} & k_{2,3} & 0 & 0 & & & & & & & & & & 0 \\
0 & k_{3,2} & k_{3,3} & k_{3,4} & 0 & 0 & & & & & & & & & 0 \\
0 & 0 & k_{4,3} & k_{4,4} & k_{4,5} & 0 & 0 & & & & & & & & 0 \\
0 & 0 & 0 & k_{5,4} & k_{5,5} & k_{5,6} & 0 & 0 & & & & & & & 0 \\
0 & & 0 & 0 & k_{6,5} & k_{6,6} & k_{6,7} & 0 & 0 & & & & & & 0 \\
0 & & & 0 & 0 & k_{7,6} & k_{7,7} & k_{7,8} & 0 & k_{7,10} & & & & & 0 \\
0 & & & & 0 & 0 & k_{8,7} & k_{8,8} & k_{8,9} & 0 & 0 & & & & 0 \\
0 & & & & & 0 & 0 & k_{9,8} & k_{9,9} & 0 & 0 & k_{9,12} & & & 0 \\
0 & & & & & & k_{10,7} & 0 & 0 & k_{10,10} & k_{10,11} & 0 & 0 & & 0 \\
0 & & & & & & & 0 & 0 & k_{11,10} & k_{11,11} & k_{11,12} & 0 & 0 & 0 \\
0 & & & & & & & & k_{12,9} & 0 & k_{12,11} & k_{12,12} & k_{12,13} & 0 & 0 \\
0 & & & & & & & & & 0 & 0 & k_{13,12} & k_{13,13} & k_{13,14} & k_{13,15} \\
0 & & & & & & & & & & 0 & 0 & k_{14,13} & k_{14,14} & 0 \\
0 & 0 & 0 & 0 & 0 & 0 & 0 & 0 & 0 & 0 & 0 & 0 & k_{15,13} & 0 & k_{15,15}
\end{bmatrix} \tag{4}$$

while the elements of the matrix of damping take the form:

$$c_{1,1} = c_{MK}; \quad c_{1,2} = -c_{MK}$$

$$c_{2,1} = -c_{MK}; \quad c_{2,2} = c_{MK} + c_K^{(1)}; \quad c_{2,3} = -c_K^{(1)}$$

$$c_{3,2} = -c_K^{(1)}; \quad c_{3,3} = c_K^{(1)} + c_{MI}; \quad c_{3,4} = -c_{MI}$$

$$c_{4,3} = -c_{MI}; \quad c_{4,4} = c_{MI} + c_K^{(2)}; \quad c_{4,5} = -c_K^{(2)}$$

$$c_{5,4} = -c_K^{(2)}; \quad c_{5,5} = c_K^{(2)} + c_{K1}; \quad c_{5,6} = -c_{K1}$$

$$c_{6,5} = -c_{K1}; \quad c_{6,6} = c_{K1} + c_{12}; \quad c_{6,7} = -c_{12}$$

$$c_{7,6} = -c_{12}; \quad c_{7,7} = c_{12} + c_{23}^{(1)} + c_{23}^{(2)}; \quad c_{7,8} = -c_{23}^{(1)}; \quad c_{7,10} = -c_{23}^{(2)}$$

$$c_{8,7} = -c_{23}^{(1)}; \quad c_{8,8} = c_{23}^{(1)} + c_{34}^{(1)}; \quad c_{8,9} = -c_{34}^{(1)}$$

$$c_{9,8} = -c_{34}^{(1)}; \quad c_{9,9} = c_{34}^{(1)} + c_{45}^{(1)}; \quad c_{9,12} = -c_{45}^{(1)}$$

$$c_{10,7} = -c_{23}^{(2)}; \quad c_{10,10} = c_{23}^{(2)} + c_{34}^{(2)}; \quad c_{10,11} = -c_{34}^{(2)}$$

$$c_{11,10} = -c_{34}^{(2)}; \quad c_{11,11} = c_{34}^{(2)} + c_{45}^{(2)}; \quad c_{11,12} = -c_{45}^{(2)}$$

$$c_{12,9} = -c_{45}^{(1)}; \quad c_{12,11} = -c_{45}^{(2)}; \quad c_{12,12} = c_{45}^{(1)} + c_{45}^{(2)} + c_{56}; \quad c_{12,13} = -c_{56}$$

$$c_{13,12} = -c_{56}; \quad c_{13,13} = c_{56} + c_{6G}^{(1)} + c_{6G}^{(2)}; \quad c_{13,14} = -c_{6G}^{(1)}; \quad c_{13,15} = -c_{6G}^{(2)}$$

$$c_{14,13} = -c_{6G}^{(1)}; \quad c_{14,14} = c_{6G}^{(1)}$$

$$c_{15,13} = -c_{6G}^{(2)}; \quad c_{15,15} = c_{6G}^{(2)}$$

and the elements of the matrix of rigidity look as follows:

$$k_{1,1} = k_{MK}; \quad k_{1,2} = -k_{MK}$$

$$k_{2,1} = -k_{MK}; \quad k_{2,2} = k_{MK} + k_K^{(1)}; \quad k_{2,3} = -k_K^{(1)}$$

$$k_{3,2} = -k_K^{(1)}; \quad k_{3,3} = k_K^{(1)} + c_{MI}; \quad k_{3,4} = -k_{MI}$$

$$k_{4,3} = -k_{MI}; \quad k_{4,4} = k_{MI} + k_K^{(2)}; \quad k_{4,5} = -k_K^{(2)}$$

$$k_{5,4} = -k_K^{(2)}; \quad k_{5,5} = k_K^{(2)} + k_{K1}; \quad k_{5,6} = -k_{K1}$$

$$k_{6,5} = -k_{K1}; \quad k_{6,6} = k_{K1} + k_{12}; \quad k_{6,7} = -k_{12}$$

$$k_{7,6} = -k_{12}; \quad k_{7,7} = k_{12} + k_{23}^{(1)} + k_{23}^{(2)}; \quad k_{7,8} = -k_{23}^{(1)}; \quad k_{7,10} = -k_{23}^{(2)}$$

$$k_{8,7} = -k_{23}^{(1)}; \quad k_{8,8} = k_{23}^{(1)} + k_{34}^{(1)}; \quad k_{8,9} = -k_{34}^{(1)}$$

$$k_{9,8} = -k_{34}^{(1)}; \quad k_{9,9} = k_{34}^{(1)} + k_{45}^{(1)}; \quad k_{9,12} = -k_{45}^{(1)}$$

$$k_{10,7} = -k_{23}^{(2)}; \quad k_{10,10} = k_{23}^{(2)} + k_{34}^{(2)}; \quad k_{10,11} = -k_{34}^{(2)}$$

$$k_{11,10} = -k_{34}^{(2)}; \quad k_{11,11} = k_{34}^{(2)} + k_{45}^{(2)}; \quad k_{11,12} = -k_{45}^{(2)}$$

$$k_{12,9} = -k_{45}^{(1)}; \quad k_{12,11} = -k_{45}^{(2)}; \quad k_{12,12} = k_{45}^{(1)} + k_{45}^{(2)} + k_{56}; \quad k_{12,13} = -k_{56}$$

$$k_{13,12} = -k_{56}; \quad k_{13,13} = k_{56} + k_{6G}^{(1)} + k_{6G}^{(2)}; \quad k_{13,14} = -k_{6G}^{(1)}; \quad k_{13,15} = -k_{6G}^{(2)}$$

$$k_{14,13} = -k_{6G}^{(1)}; \quad k_{14,14} = k_{6G}^{(1)}$$

$$k_{15,13} = -k_{6G}^{(2)}; \quad k_{15,15} = k_{6G}^{(2)}$$

A vector of external forces is created by the moments of forces acting on the respective masses:

$$\mathbf{Q} = \left[M_M(t), 0, 0, 0, 0, 0, 0, 0, 0, 0, 0, 0, 0, -M_{OB}^{(1)}(t), -M_{OB}^{(2)}(t) \right]^T \tag{5}$$

where $M_M(t) = M_e(t)$ is electromagnetic driving torque reached by an electric motor, and $M_{OB}^{(1)}(t)$ and $M_{OB}^{(2)}(t)$ – the moment of load forces of, respectively: the left and right cutting head being an excitation of vibrations in the drive of cutting heads. The time curves of this excitation are determined using an original simulation model allowing to simulate, with a computer, a process of cutting a heading face of the drilled heading (Cheluszka, 2015).

The vector of the coordinates **q** has the following form here:

$$\mathbf{q} = \left[\varphi_M, \varphi_K^{(11)}, \varphi_K^{(12)}, \varphi_K^{(21)}, \varphi_K^{(22)}, \varphi_1, \varphi_2, \varphi_3^{(1)}, \varphi_4^{(1)}, \varphi_3^{(2)}, \varphi_4^{(2)}, \varphi_5, \varphi_6, \varphi_G^{(1)}, \varphi_G^{(2)} \right]^T \tag{6}$$

2.2. Modelling the dynamics of a converter system with a double squirrel-cage drive motor and a frequency converter with pulse width modulation (PWM)

A drive of boom roadheader cuttings heads, for which a dynamic model was constructed, is equipped with an asynchronous double squirrel-cage AC motor. Different solutions for a simulation model of an induction motor can be found in literature (Pedra et al., 2009), (Xiang et al., 2010).

The most often used solution is a circumferential mathematical model of a single squirrel-cage induction motor recorded by means of spatial vectors with simplification assumptions (Matlab on-line documentation, 2016). This creates significant problems when determining such model's parameters, as it is impossible to represent appropriately the characteristics delivered by a motor manufacturer with five parameters of an equivalent circuit diagram. Much more accurate representation is possible with seven parameters of an equivalent circuit diagram of a double squirrel-case motor. A model of a dynamic three-phase double squirrel-cage induction motor was formulated in a coordinate system with two axes dq rotating in the same direction as the motor rotor. The following was used as input signals:

- temporary values of three phase voltages $u_a(t)$, $u_b(t)$, $u_c(t)$,
- temporary value of load torque;

and the following was used as output signals:

- electromagnetic moment $M_e(t)$,
- temporary values of three-phase currents of stator $i_a(t)$, $i_b(t)$, $i_c(t)$;
- angular speed of motor shaft $\dot{\varphi}_M(t)$.

It is also possible to control the waveforms of other motor "internal" signals, such as:

- magnetic fluxes associated with stator and rotor windings;
- electric power at motor terminals;

torques and currents of the both rotor cages.

A differential equation describing the curve of the stator flux is as follows:

$$\mathbf{u_s} = R_s \mathbf{i_s} + \frac{d}{dt}\mathbf{\Psi_s} + j\dot{\varphi}_0 \mathbf{\Psi_s} \tag{7}$$

where:

R_S — stator resistance,
$\dot{\varphi}_0$ — synchronous speed.

The spatial vectors $\mathbf{u_s}$, $\mathbf{i_s}$, $\mathbf{\Psi_s}$ can be presented as complex numbers. Two equations are obtained by separating the equation (7) into a real part and an imaginary part:

$$\begin{cases} u_{sd} = R_s i_{sd} + \dfrac{d\Psi_{sd}}{dt} - \dot{\varphi}_0 \Psi_{sq} \\ u_{sq} = R_s i_{sq} + \dfrac{d\Psi_{sq}}{dt} + \dot{\varphi}_0 \Psi_{sd} \end{cases} \tag{8}$$

The equations describing rotor fluxes have a simpler form:

$$\mathbf{0} = R_{w1}\mathbf{i_{w1}} + \frac{d}{dt}\mathbf{\Psi_{w1}} \tag{9}$$

$$\mathbf{0} = R_{w2}\mathbf{i_{w2}} + \frac{d}{dt}\mathbf{\Psi_{w2}} \tag{10}$$

where:

R_{W1}, R_{W2} — resistance of particular rotor cages.

The dependencies between flux linkages of the windings of the stator and both rotor cages can be recorded as algebraic matrix equations:

$$\begin{bmatrix} \Psi_{sd} \\ \Psi_{w1d} \\ \Psi_{w2d} \end{bmatrix} = \begin{bmatrix} M + L_s & M & M \\ M & M + L_{w1} & M \\ M & M & M + L_{w2} \end{bmatrix} \cdot \begin{bmatrix} i_{sd} \\ i_{w1d} \\ i_{w2d} \end{bmatrix} \tag{11}$$

and

$$\begin{bmatrix} \Psi_{sq} \\ \Psi_{w1q} \\ \Psi_{w2q} \end{bmatrix} = \begin{bmatrix} M + L_s & M & M \\ M & M + L_{w1} & M \\ M & M & M + L_{w2} \end{bmatrix} \cdot \begin{bmatrix} i_{sq} \\ i_{w1q} \\ i_{w2q} \end{bmatrix} \tag{12}$$

where:

M — mutual inductance between stator and rotor,
L_s — stator inductance,
L_{w1}, L_{w2} — inductance of particular rotor cages.

By knowing the values of fluxes $[\Psi_{sd}, \Psi_{sq}]^T$, $[\Psi_{w1d}, \Psi_{w1q}]^T$, $[\Psi_{w2d}, \Psi_{w2q}]^T$, the components of currents of stator windings i_{sd}, i_{sq} and rotor windings i_{w1d}, i_{w2d}, i_{w1q}, i_{w2q} generating them can be determined.

Electromagnetic moment is determined based on the values of stator fluxes and currents (the values which are easiest to access or restore in a measuring and control circuit) according to the formula:

$$M_e(t) = \frac{3}{2} p_b \left[\Psi_{sd}(t) i_{sq}(t) - \Psi_{sq}(t) i_{sd}(t) \right] \tag{13}$$

where: p_b — pairs of motor poles.

In order to simulate a model of a motor formulated with *dq* coordinates, a control signal, that is phase voltages *abc* being an output signal from a frequency converter, has to be transferred into such an input circuit. This is done by successive Clarke (Clarke, 1943) and Park (Park, 1929) transformations.

A frequency converter with the spatial vector method (Zhou & Wang, 2002) was used for the purpose of angular speed adjustment of cutting heads. It was modelled as a source of three symmetric three-phase voltages with adjustable amplitude and frequency. A two-phase description of a three-phase voltages circuit was applied with the use of a spatial vector defined with a Clarke transformation (Clarke, 1943):

$$\begin{bmatrix} v_\alpha(t) \\ v_\beta(t) \\ v_\gamma(t) \end{bmatrix} = \begin{bmatrix} 1 & -\frac{1}{2} & -\frac{1}{2} \\ 0 & \frac{\sqrt{3}}{2} & -\frac{\sqrt{3}}{2} \\ \frac{1}{2} & \frac{1}{2} & \frac{1}{2} \end{bmatrix} \cdot \begin{bmatrix} v_a(t) \\ v_b(t) \\ v_c(t) \end{bmatrix} \tag{14}$$

A complex spatial vector of voltage **V** is defined as:

$$\mathbf{V(t)} = v_\alpha(t) + jv_\beta(t) \tag{15}$$

This method is commonly used for describing rotating AC electrical machines, as it decreases the number of differential equations and enables to use complex numbers (if the real part is assigned to α component, and an imaginary part to β component).

In case of a symmetric circuit of three-phase sinusoidal voltages (e.g. supply voltage) with the effective (interphase) value U, the end of a spatial vector **V** draws a circle with the radius $\sqrt{\frac{2}{3}}U$. However, in case of a transistor frequency converter (Fig. 3), a circuit of three-phase output voltages may only assume 8 discreet values. Any spatial vector (from the range within a hexagon determined by the ends of vectors $\mathbf{V}_1 ... \mathbf{V}_6$) can be generated as a sequence of impulses with an appropriate average value. The following can be recorded for the vector $\mathbf{V_{zad}}$ between the vectors $\mathbf{V_1}$ and $\mathbf{V_2}$ presented in Fig. 4 (by designating the period of modulation as T_m):

$$\mathbf{V_{zad}} = \mathbf{V_1}\frac{T_1}{T_m} + \mathbf{V_2}\frac{T_2}{T_m} + \mathbf{V_0}\frac{T_0}{T_m} \tag{16}$$

where:

$\mathbf{V_0}$ — means one of two zero vectors $\mathbf{V_7}$ or $\mathbf{V_8}$.

T_1, T_2, T_0 — means output voltage pulse duration corresponding to output voltage vectors $\mathbf{V_1}, \mathbf{V_2}$ and $\mathbf{V_0}$.

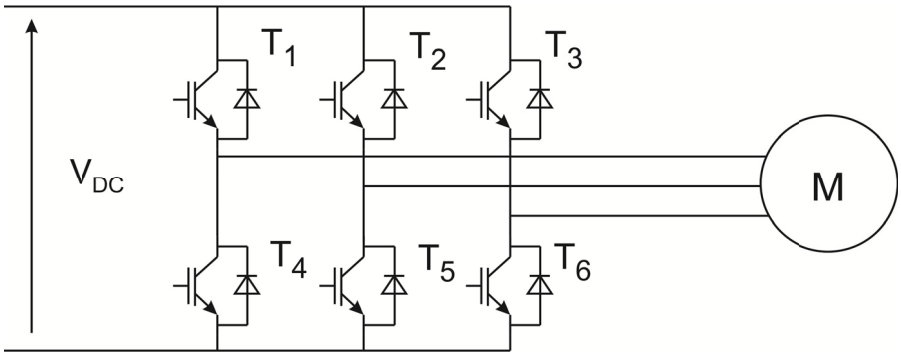

Fig. 3. Symbols of inverter transistors with pulse width modulation

3. Implementation of the simulation model of the drive system of the boom-type roadheader cutting heads in matlab/simulink environment

A simulation model of a drive system of roadheader cutting heads comes as an integrated system: the converter system – asynchronous double squirrel-cage motor – power transmission system – cutting heads (Fig. 5÷8). The dynamics of a roadheader cutting system equipped with a

converter system in the established mathematical model are described with twenty-two differential equations – seven equations of the first order (inverter-asynchronous motor) and fifteen equations of the second order (power transmission system). In order to solve this system of equations, the simulation modules reflecting its particular elements create a structure of a programme created in Matlab/Simulink environment. The equations describing the motion of masses in a model and the time curves of characteristic parameters of a frequency converter – drive motor system, are integrated numerically with the Dormand-Prince method with a variable step. Voltage signals from the inverter output (apart from other signals – e.g. of angular speed) become input signals for a electric engine model (marked as dark grey in Fig. 5). Scalar frequency converter control is

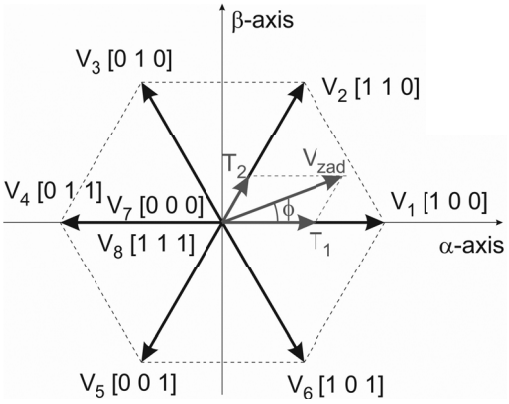

Fig. 4. Graphical interpretation of the method of restoring the set value of the output voltage vector as a weighted sum of neighbouring vectors

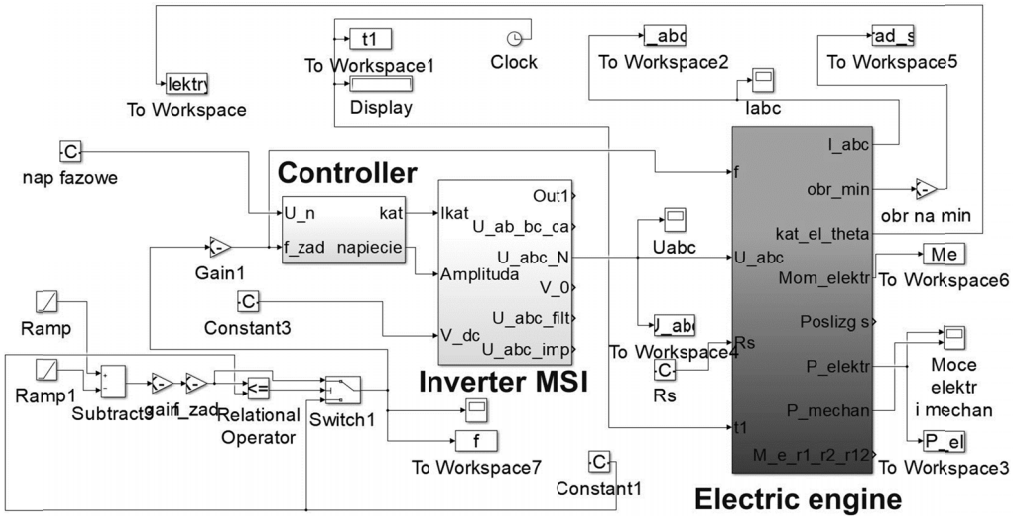

Fig. 5. Block diagram of a model of a drive system of roadheader cutting heads with scalar control of the converter system implemented in Matlab/Simulink environment

carried out in this model while maintaining a constant voltage-to-frequency ratio (U/f = const). This ensures, within the considered range of angular speeds, the stabilisation of stator flux values. The established simulation model was tested in a system working without feedback and in a system with feedback and with a PID controller ensuring angular speed stabilisation for load variations. The equations of motion of masses in a power transmission system are implemented from the "Toothed gear" block (Fig. 6). The differential equations describing a vibrating motion in a model of this system create the structure of fifteen blocks linked by signals (Fig. 7), in which their numerical integration is performed (Fig. 8) and a block in which an external load (Moment of load forces) is applied.

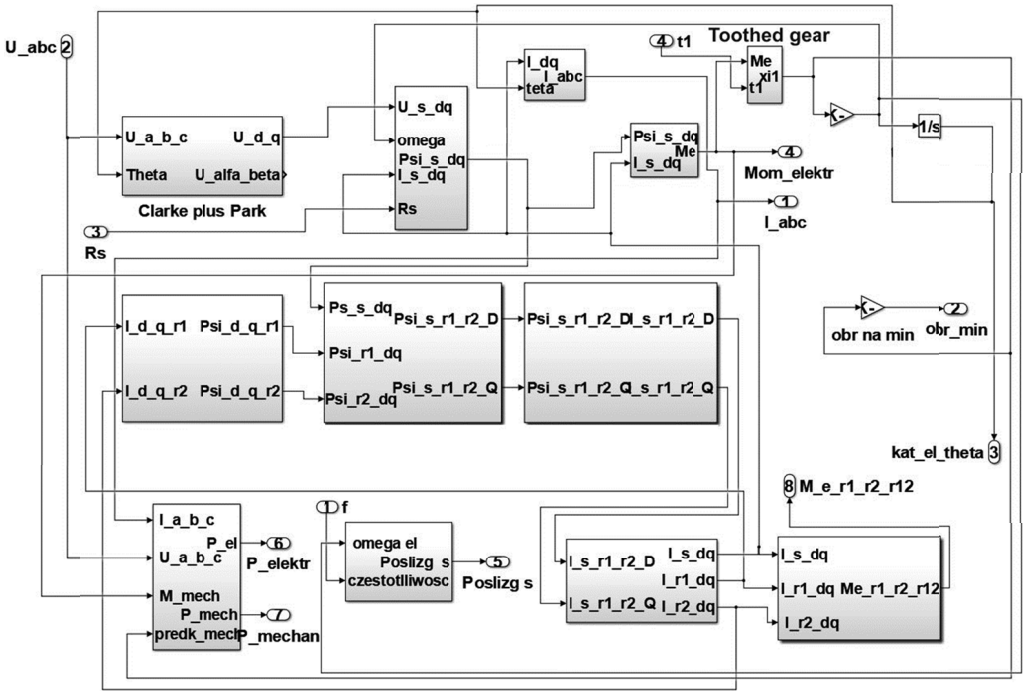

Fig. 6. Block diagram of the "Double squirrel-cage motor" section in Matlab/Simulink environment

One of the essential elements decisive for the correct work of a simulation model is a block of selection of an inverter output voltage vector sector (Suresh et al., 2014). It was carried out with a number of standard logical operations (comparison and conjunction). The so obtained sector number, ranging between 1 to 6 (Fig. 9a), next becomes an index in a selection table of vector control signals fundamental for the sequence of making and breaking inverter transistors. The duration of particular voltage pulses is determined in a modulator block. Output pulses (Fig. 9b) are generated using a synchronisation block generating a sawtooth signal (Fig. 9c) with frequency equal to PWM modulation frequency. The pulses are generated by blocks performing relevant comparisons during one period. An output filter of the inertial character is placed at the inverter output. It corresponds to LC filters incorporated in output circuits (limiting overvoltages in cable

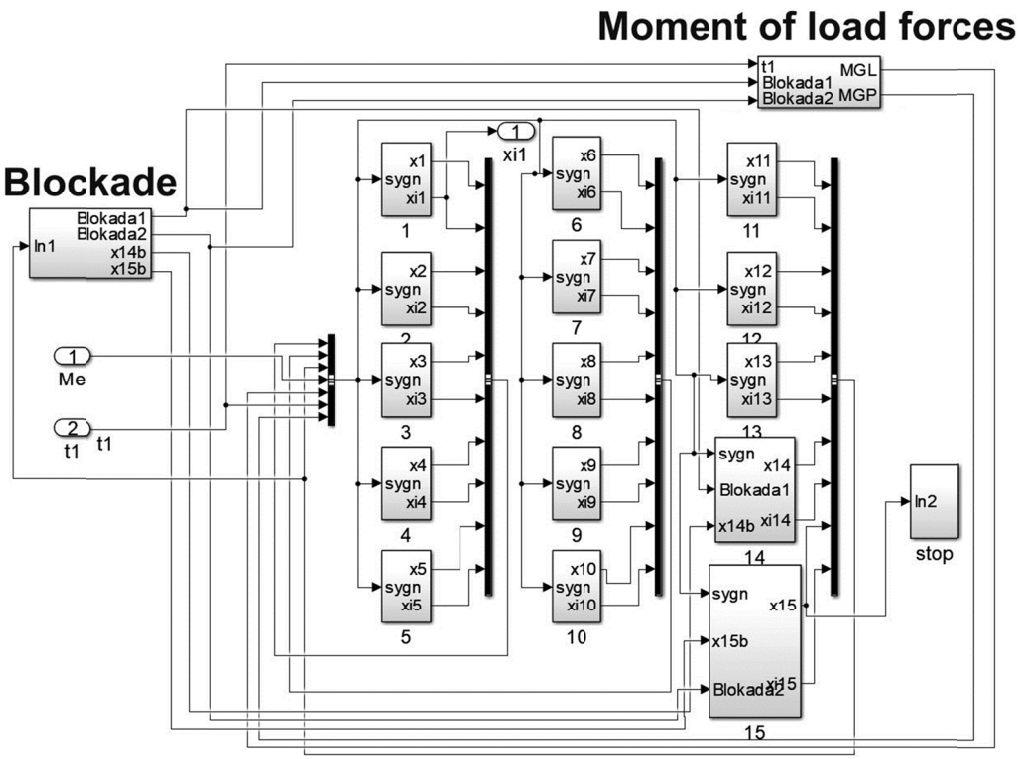

Fig. 7. Block diagram of the "Toothed gear" section in Matlab/Simulink environment

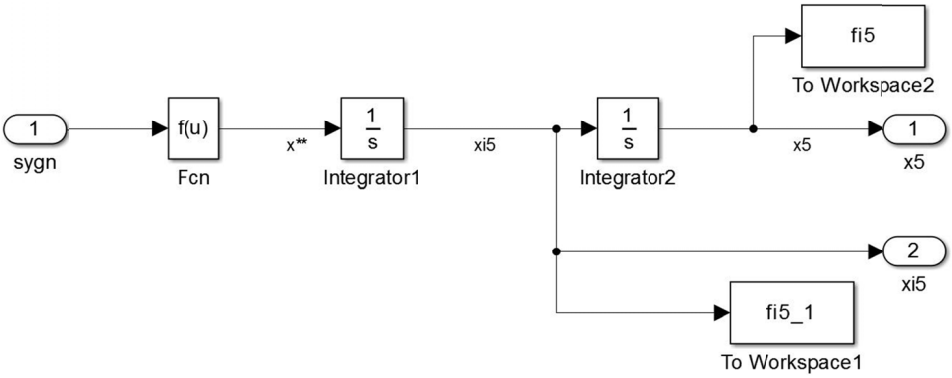

Fig. 8. Structure of numerical integration modules of differential equations of motion in a physical model of the system of power transmission onto cutting heads in Matlab/Simulink environment

line). Its task is to smooth the voltage waveform (Fig. 9d). This makes it easier to simulate the phenomena occurring in a double squirrel-case motor by allowing to considerably increase the simulation speed (extend an integration step of differential equations).

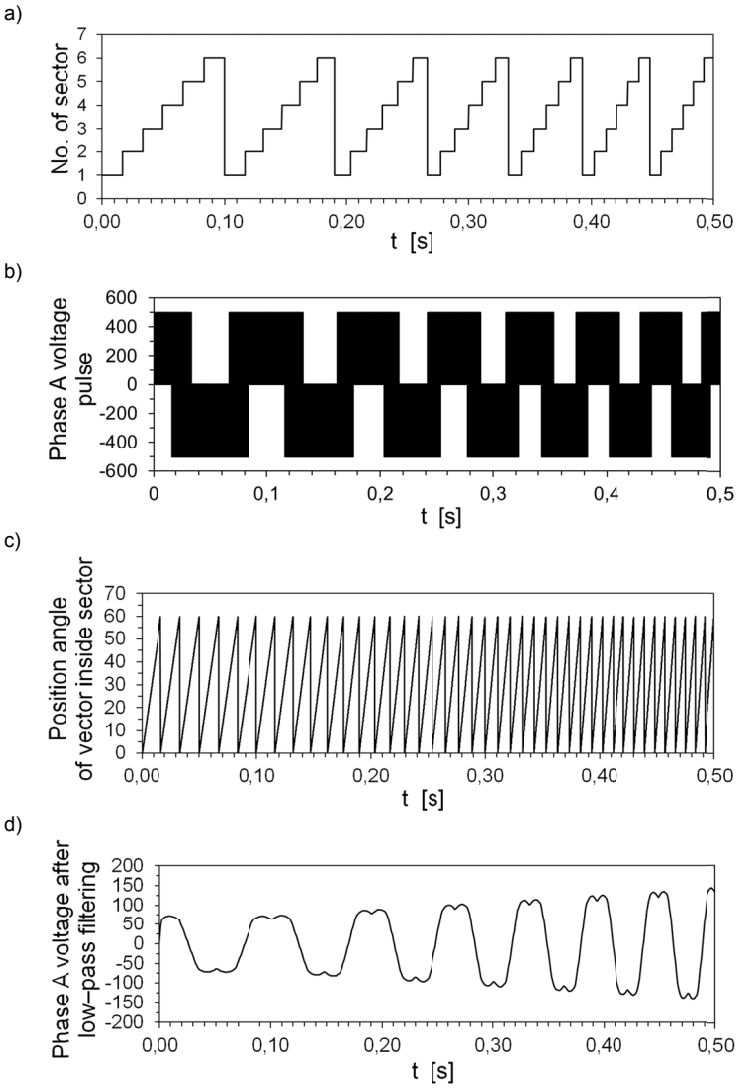

Fig. 9. Curves of inverter control and output signals at a motor start-up

The set frequency to be reached by a frequency converter f_{ref} during simulated drive start-up is determined in a function of the set angular speed of cutting heads, at which a cutting process is to be performed, with the following proportions:

$$f_{ref} = f_n \frac{\dot{\varphi}_{Gref}}{\dot{\varphi}_{Gn}} \tag{17}$$

where:

f_n — rated frequency of supply network (f_n =50 Hz),

$\dot{\varphi}_{G\,ref}$ — set value of angular speed of cutting heads,
$\dot{\varphi}_{Gn}$ — nominal angular speed of cutting heads (for the applied drive and toothed gear in a cutting system of the studied roadheader $\dot{\varphi}_{Gn}$ = 9.24 rad/s).

4. Examples of the results of computer simulations

Figures 10 and 11 show the results of a simulation of a driver system start-up of cutting heads for two different values of supply voltage frequency f_{ref}: 50 Hz and 25 Hz. Upon the driver system start-up, the inverter works with the minimum frequency of f_{min} = 10 Hz (Fig. 10a and 11a – green line). As the drive start-up is done at idle run, a drive motor upon start is loaded mainly with the forces of inertia of the accelerated masses of the system. As a result, after sudden growth

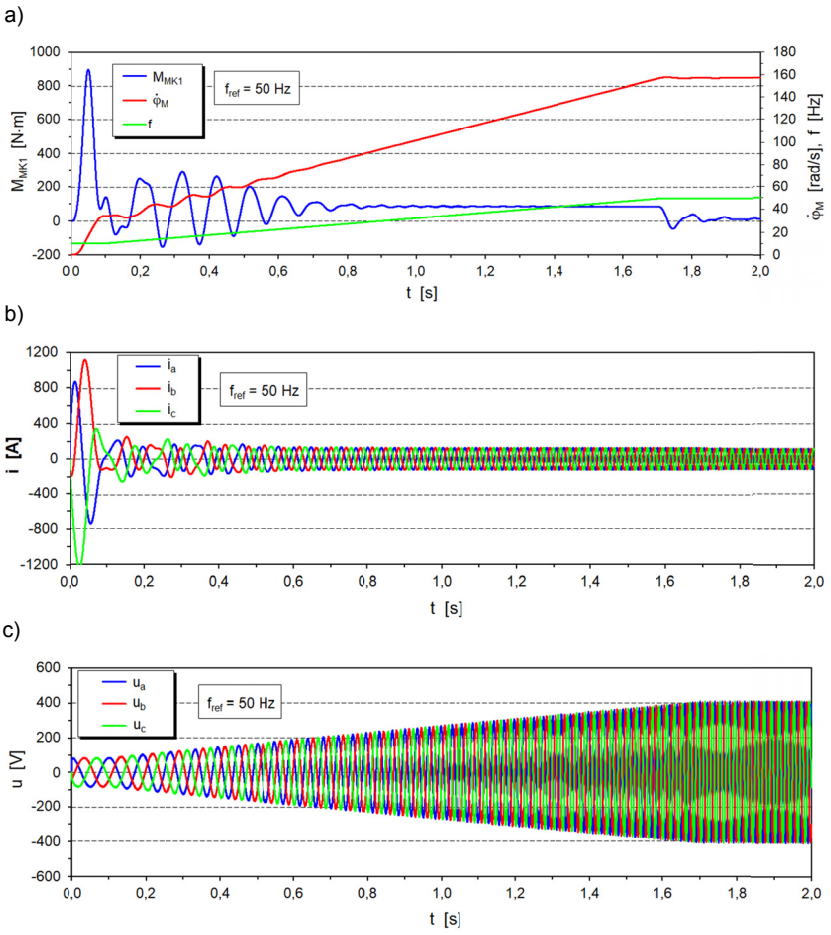

Fig. 10. Time characteristics obtained while simulating the start-up of the cutting heads drive for f_{ref} = 50 Hz: a) curve of the torque on the motor shaft (blue line) and angular speed of a motor rotor (red line), b) curve of temporary values of supply current in particular phases, c) curve of temporary values of phase voltage

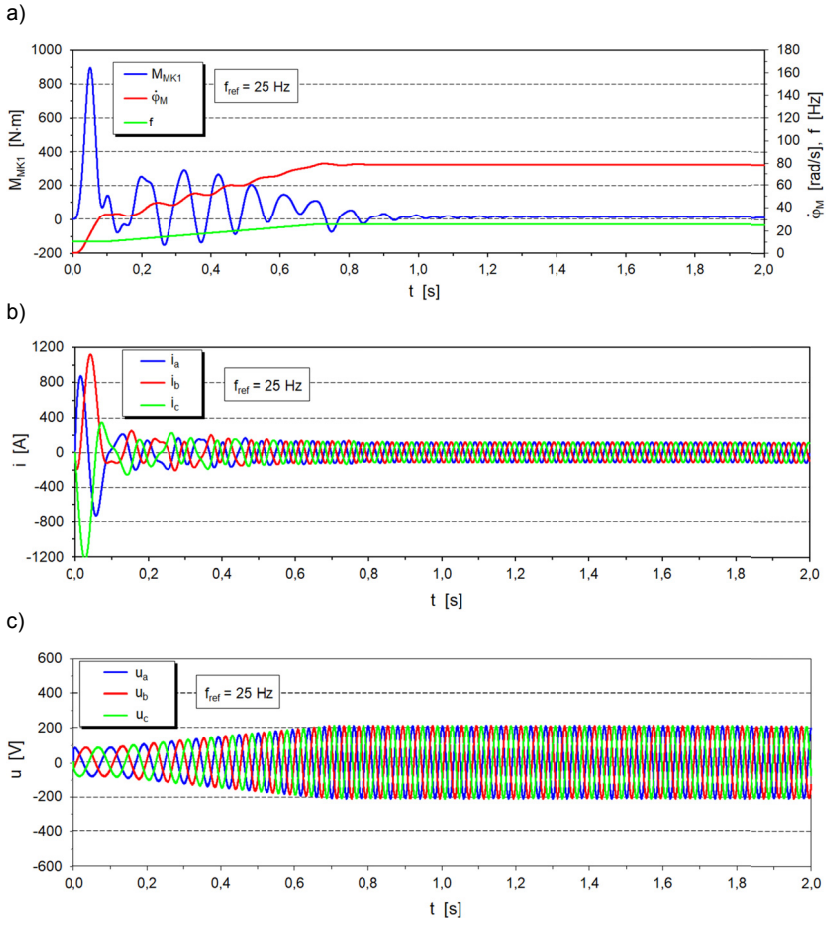

Fig. 11. Time characteristics obtained while simulating the start-up of the cutting heads drive for f_{ref} = 25 Hz: a) curve of the torque on the motor shaft (blue line) and angular speed of a motor rotor (red line), b) curve of temporary values of supply current in particular phases, c) curve of temporary values of phase voltage

in a dynamic load on the motor shaft up to 900 N×m, rapid load decrease is seen (blue line). As voltage frequency rises, thus the angular speed of rotating masses, dynamic moment oscillations on the motor shaft decrease quickly. After the time of 0.8 s, the values of this load stabilise at the level of 90 N×m. After reaching the set angular speed value (Fig. 10a – red line) – after 1.7 s of simulation – a motor load falls to values near zero, resulting only from the assumed resistance of the motion of rotating parts.

Upon drive start-up, the current in particular phases reaches even up to 1200 A (Fig. 10b). As the angular speed of cutting heads rises, the current-carrying capacity of the supply voltage falls quickly. After about 0.6 s of simulation, the peak values of supply current in the particular phases reach the level of 125 A. As angular speed adjustment of a motor is carried out with the constant value of *U*/*f*, the peak values of phase voltages rise proportionally to the frequency of the set characteristic of the referencing unit in the range of about 80 to 400 V (Fig. 10c).

If voltage frequency was reduced to the half of the rated value (f_{ref} = 25 Hz), the start-up time was about 0.7 s. This time was, however, too short to extinguish torque vibrations on the motor shaft and the angular speed of the rotor. The load on the motor shaft was therefore stabilised already during a steady-state motion of a drive at idle run (Fig. 11a). After reaching the set angular speed, the peak values of current in particular phases reach the level of 115 A (Fig. 11b), with the peak value of phase voltage of about 200 V (Fig. 11c).

The character of the curve and the magnitude of excitation of vibrations in a drive of working units of mining cutting machines have a decisive effect on the dynamic load in this system. Figures 12 and 13 show the time characteristics obtained from a computer simulation of dynamics of the cutting heads' drive when performing the cutting process. The simulations covered time intervals lasting about 5 seconds, corresponding to seven – for f_{ref} = 50 Hz and about three – for

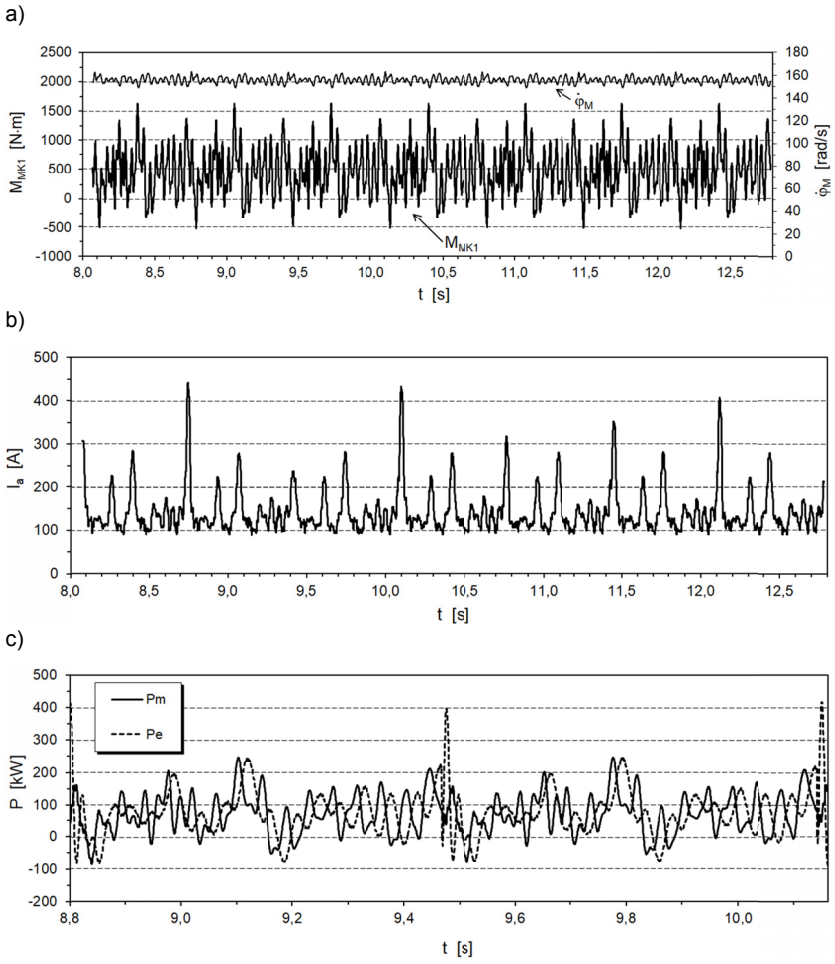

Fig. 12. Time curves of: a) torque on the motor shaft (thick line) and angular speed of motor rotor (thin line), b) effective value of current in phase A, c) mechanical power (continuous line) and electric power (intermittent line), obtained from the simulation of cutting process for f_{ref} = 50 Hz

f_{ref} = 25 Hz revolutions of the cutting heads. The cutting of the rock with the average compressive strength of R_c = 55 MPa with cutting heads equipped with 40 picks was simulated here. The cutting of a layer with the height of h = 0.15 m and the web of z = 0.14 m was considered with the advancement speed of the cutting heads in the plane parallel to the floor of v_{OW} = 0.05 m/s.

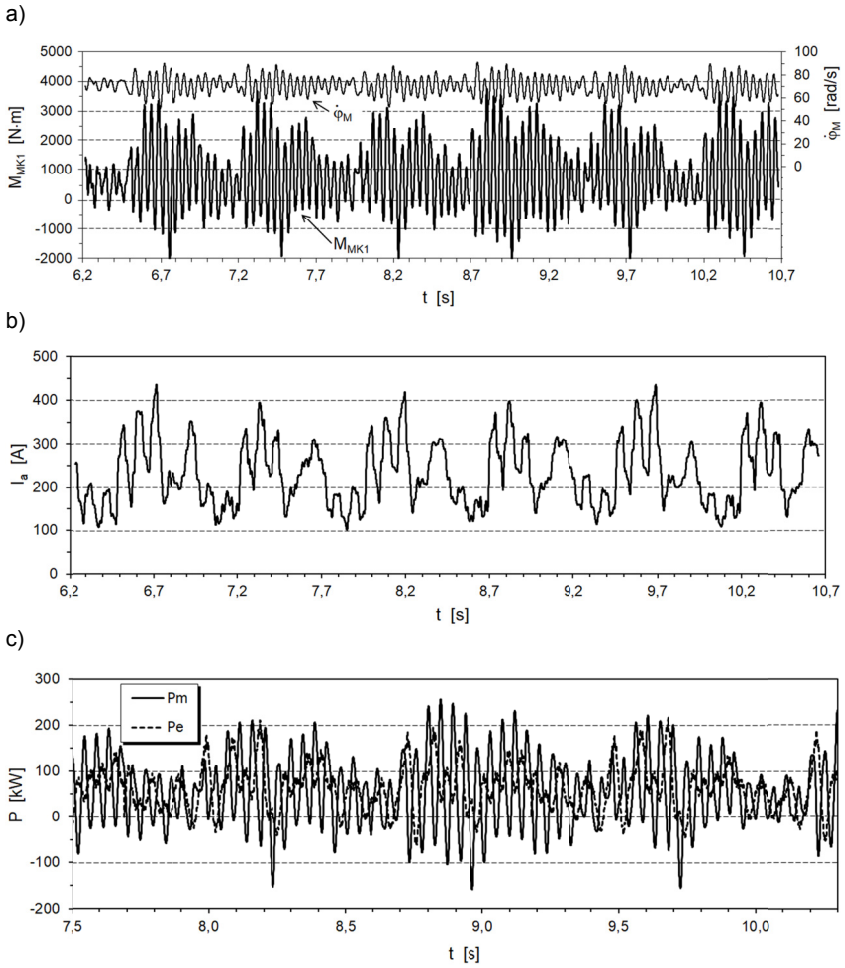

Fig. 13. Time curves of: a) torque on the motor shaft (thick line) and angular speed of motor rotor (thin line), b) effective value of current in phase A, c) mechanical power (continuous line) and electric power (intermittent line), obtained from the simulation of cutting process for f_{ref} = 23 Hz

For the angular speed of the cutting heads of $\dot{\varphi}_G$ = 9.24 rad/s (for f_{ref} = 50 Hz), the drive motor is loaded with variable torque with the average value of 468 N×m (Fig. 12a – thick line). The average load is therefore 60% of the motor's nominal torque (M_n = 851 N×m). The amplitude of torque vibrations on the motor shaft (understood as the variability range of this load) exceeds 2000 N×m here. A peak value of this load reaches here up to 1635 N×m. This value for

the modelled drive motor is much lower than the critical value M_K (M_K/M_n = 3,5), as a result of which the working point is situated on the stable part of its mechanical characteristics. The average angular speed of a drive motor rotor is at the level of 156 rad/s (thin line), whereas its vibration amplitude is 14 rad/s.

The average value of the effective value of a current curve in particular phases is at the level of 145 A (Fig. 12b). It, thus, accounts for about 77% of rated current. Peaks with the value of up to 440 A are, however, visible in the current load curve (about 2.3-time the value of rated current). This is a result of the reaction of the motor power supply system to dynamic loads, subject to which is the drive of cutting heads during the simulated rock cutting for the set parameter values of this process. The average electric power drawn from a supply network in the analysed case is 76.1 kW (about 60% of the motor rated power) – intermittent line in Fig. 12c. Temporary values reach, however, even 420 kW (nearly 3 times the nominal value). The variability range of the electric power curve is high here. The average mechanical power reached by the driver motor equals 73 kW (continuous line in Fig. 12c). The peak values of the curve of this power in the analysed time interval account for nearly 250 kW. The time curves of electric and mechanical power are distinct for a clear phase shift. The average drive motor efficiency is high in this case and accounts for 95.4%. The average energy consumption of cutting, understood as the quotient of the power consumed for the implementation of the cutting process and its efficiency, is 20.0 kWh/m^3 here.

The character of a dynamic load curve of a cutting heads drive is clearly different in case of the second of the considered set frequencies of motor supply voltage in the cutting system (f_{ref} = 25 Hz). Considering the load condition of the converter supply system of the motor of the studied drive, the supply voltage frequency has decreased to f = 23 Hz. As a result, the simulated cutting was performed for slightly lower angular speed of cutting heads than assumed. The average angular speed of the cutting heads was, however, 4.28 rad/s here and was 8% smaller than the defined value. The average value of torque on the motor shaft represents here a nominal level of the considered electric motor (Fig. 13a – thick line). Peak values are very high though, as they exceed 3700 N×m. Similarly, a dynamic load amplitude on the motor shaft is high, as it is as much as 6040 N×m. Nevertheless, the motor is not stalling, the angular speed of its rotor has only decreased. This is a result of the working control system of the inverter. The average angular speed of the motor rotor in the analysed case is 70.6 rad/s, whereas its vibration amplitude is nearly 4 times higher than the case considered earlier (thin line).

The effective value of the current in particular phases is changing in the range of 103 to about 440 A (Fig. 13b). The peak values of this current are 2.3 times higher than the rated supply current value of the considered motor. The average value is 24% higher than the nominal value, as it is 233 A. The average mechanical power determined on the drive motor shaft, necessary to perform cutting with the set parameter values of this process, is 55 kW (Fig. 13c – continuous line). The average electric power on the other hand is 64 kW (intermittent line). It reaches the level of the rated power developed by the drive motor for the considered supply voltage frequency. The dynamics of the electric power curve are different here (the electric power curve amplitude is clearly smaller here than the mechanical power curve amplitude). The motor efficiency is slightly lower in this case, as it is 90.2%. The average energy consumption of cutting equals to 16.4 kWh/m^3.

The presented examples of computer simulations clearly show how large is the effect of the cutting process parameters values on the dynamic load of a cutting heads drive, its supply system and process energy consumption. The stereometry of cutting heads (the number and manner of

arranging picks and its side surface) is also important here. If the angular speed of the investigated cutting heads was reduced by a half, the resulting energy consumption of cutting has decreased by nearly 20% while maintaining the values of other cutting process parameters. The dynamic loads of their drive were largely increased as a result, however, in a particular vibration amplitude.

5. Conclusions

A dynamic model of a drive system of boom-type roadheader cutting heads presented in this work provides broad investigation possibilities to analyse the dynamic phenomena accompanying the execution of the cutting process. While developing the model, the cutting system was approached as a whole – as a complex mechatronic object. An asynchronous double squirrel-cage electric motor supplied from a controlled power supply source (frequency converter), a power transmission system in the form of a multistage toothed gear and a working unit (cutting heads) were considered in its structure. The work of a drive system for different angular speeds of cutting heads can be simulated by modelling a converter system. This is a starting point for optimising, for the given conditions of executing the cutting process, the values of the parameters of the process, including the angular speed of cutting heads. At a later stage, the model will be extended to include, in particular, a vector control of the converter system.

The results of the comparative analysis of dynamic characteristics, obtained from the computer simulations and measurements performed on a test station created for this purpose (Fig. 1), indicate that the model developed is helpful for simulation tests. Once the adequacy of the presented model is confirmed (verified), it will be employed for simulation tests aimed at the determination of adjustment characteristics of a cutting system of a boom-type roadheader.

Acknowledgements

The work has been implemented under the research project titled "*Control of roadheader cutting heads movement for reduction of energy consumption of mining and dynamic loads*" co–financed by the Polish National Centre for Research and Development under the Applied Research Projects (agreement no. PBS3/B2/15/2015).

References

Bishop R.H. (ed.), 2002. *The Mechatronics Handbook*. CRC Press, Boca Raton – London – New York – Washington, D.C.

Cheluszka P., 2015. *Modeling of the geometry of cuts for purpose of the computer simulation of a point-attack picks cutting process*. Technicka Diagnostika, **24**, 1, 66-74.

Clarke E., 1943. *Circuit Analysis of A-C Power Systems*. Symmetrical and related components. Wiley, New York.

Dolipski M., 1993. *Dynamic model of coal plough*. Archives of Mining Sciences, **38**, 3, 315-330.

Dolipski M., Cheluszka P., 1999. *Dynamic model of a roadheader's cutting system with incorporates transverse cutter heads*. Archives of Mining Sciences, **44**, 1, p.113-146.

Dolipski M., Cheluszka P., Sobota P., 2014. *Numerical tests of roadheader's boom vibrations*. Vibrations in Physical Systems, **26**, 65-72.

Dolipski M., Cheluszka P., Sobota P., 2015. *Investigating the simulated control of the rotational speed of roadheader cutting heads relating to the reduction of energy consumption during the cutting process*. Journal of Mining Science, **51**, 2, 298-308, DOI: 10.1134/S106273911502012X.

Hand L.N., Finch J.D., 1998. *Analytical Mechanics*. Cambridge University Press, Cambridge.

Kessler F., Siebenhofer G., Zitz A., 1989. *Untersuchung des dynamischen Verhaltens eines Doppelschneidantriebes mit Ausgleichswelle am Beispiel eines Continuous Miners*. DYNAMACH'89 Conference Proceedings, 93-105.

Matlab on-line documentation, 2016. Power_AsynchronousMachineParams. The Mathworks Inc.: MATLAB Release 2012a, available at http://www.mathworks.com.

Park R.H., 1929. *Two reaction theory of synchronous machines*. Transactions of the AIEE, 48, 716-730.

Pedra J., Candela I., Sainz L., 2009. *Modelling of squirrel-cage induction motors for electromagnetic transient programs*. IET Electr. Power Appl., **3**, 2, 111-122.

Suresh L., Mahesh K., Janardhna M., Mahesh M., 2014. *Simulation of Space Vector Pulse Width Modulation for Voltage Source Inverter using MatLab/Simulink*. Journal of Automation & Systems Engineering, 8-3, 133-140.

Wang F., Gao Y., Zhang F., 2015. *Research of trajectory tracking strategy of roadheader cutting head using ILC*. Proceedings of the 2015 Chinese Intelligent Systems Conference, **2**, 35-44.

Wei X.H., Xie M., 2012. *Dynamic Analysis on the Longitudinal Roadheader's Cutting System*. Advanced Materials Research, **619**, 160-163, DOI: 10.4028/www.scientific.net/AMR.619.160.

Xiang X., Zhuo J., Luo Z., Wang S., 2010. *Transient simulation of double-cage induction motors under power source reversal connections braking*. Proceedings of the International Conference on Electrical and Control Engineering, 4502-4505.

Zhou K.L., Wang D.W., 2002. *Relationship between space-vector modulation and three-phase carrier-based PWM*. A comprehensive analysis. IEEE Transactions on Industrial Electronics, **49**, 1, 186-192.